

# Earth and Space Science



## RESEARCH ARTICLE

10.1029/2023EA003020

### Key Points:

- This study provides the definition and catalog of wind events in four sites in the German Bight
- The events are classified according to their persistence, mean intensity, seasonality, and interannual variability
- The events' local features are analyzed and discussed in the context of the large-scale pressure systems that originated them

### Supporting Information:

Supporting Information may be found in the online version of this article.

### Correspondence to:

S. Rubinetti,  
[sara.rubinetti@awi.de](mailto:sara.rubinetti@awi.de)

### Citation:





Rubinetti, S., Fofonova, V., Arnone, E., & Wiltshire, K. H. (2023). A complete 60-year catalog of wind events in the German Bight (North Sea) derived from ERA5 reanalysis data. *Earth and Space Science*, 10, e2023EA003020. <https://doi.org/10.1029/2023EA003020>

Received 9 MAY 2023  
Accepted 30 AUG 2023

### Author Contributions:

**Conceptualization:** S. Rubinetti, V. Fofonova  
**Formal analysis:** S. Rubinetti  
**Funding acquisition:** V. Fofonova  
**Investigation:** S. Rubinetti, V. Fofonova, E. Arnone  
**Methodology:** S. Rubinetti  
**Project Administration:** V. Fofonova, K. H. Wiltshire  
**Supervision:** K. H. Wiltshire  
**Validation:** E. Arnone  
**Writing – original draft:** S. Rubinetti

## A Complete 60-Year Catalog of Wind Events in the German Bight (North Sea) Derived From ERA5 Reanalysis Data

S. Rubinetti<sup>1,2</sup> , V. Fofonova<sup>1,2</sup> , E. Arnone<sup>3,4</sup> , and K. H. Wiltshire<sup>2</sup> 

<sup>1</sup>Alfred Wegener Institute, Helmholtz Centre for Polar and Marine Research, Bremerhaven, Germany, <sup>2</sup>Alfred Wegener Institute, Helmholtz Centre for Polar and Marine Research, List/Sylt, Germany, <sup>3</sup>Department of Physics, University of Torino, Torino, Italy, <sup>4</sup>National Research Council of Italy, Institute of Atmospheric Sciences and Climate (CNR-ISAC), Torino, Italy

**Abstract** The German Bight is a shallow area in the southeastern North Sea. Atmospheric forcing, particularly wind stress, plays an essential role in the sea circulation dynamics in the area as a source of momentum and consequent driver of the variability on seasonal to interannual timescales. Westerly and SouthWesterly winds constitute the mean state of this forcing over the North Sea due to the persistent pressure gradients between the Icelandic Low and the Azores High. Consequently, the transport in the North Sea is primarily cyclonic. Nevertheless, the presence of land influences wind stress in the coastal regions (in terms of both intensity and direction). Moreover, distant locations respond differently to the action of the atmospheric pressure centers. Therefore, studies characterizing wind statistics in specific regions are mandatory for understanding and numerically simulating the sea circulation patterns in such areas. We present a detailed analysis of wind patterns in the German Bight, specifically in the Marine Protected Areas and Helgoland Island, using ERA5 reanalysis atmospheric data. We define and catalog area-specific “events” according to their typical duration and magnitude and analyze their seasonality and interannual variability. We investigate the most recurrent locations and intensities of the high- and low-pressure dipoles causing specific wind patterns over the German Bight during the different periods of the year. We show how, besides Westerly and SouthWesterly winds, NorthWesterly flows are a recurrent pattern in the area; winds from the East are less frequent but can be extremely persistent over the same site in the spring.

**Plain Language Summary** Winds significantly affect the sea circulation in the German Bight, in the southeastern part of the North Sea. Typical winds come from the West and SouthWest, causing a general anticlockwise transport in the area. However, because of the presence of land, winds in coastal regions can significantly differ from the mean flow over the North Sea basin. This study provides a definition and complete catalog of significant wind events in the German Bight, specifically in the Marine Protected Areas and Helgoland Island, selected for their socioeconomic and scientific relevance. We describe which winds are more frequent during the year since, besides the Westerly and SouthWesterly winds, those from the NorthWest are also frequent. We report which events are more intense and which have the highest probability of persisting for several days, like the Easterly winds in spring. We also show how the frequency of the events has changed in the last decades. Finally, we also show the characteristic features of the mean sea level pressure centers originating the various wind events because these local phenomena derive from atmospheric systems over a large area.

## 1. Introduction

The North Sea is a semi-enclosed basin in the North Atlantic Ocean. It is connected to the Open Ocean through the English Channel in the South and the Norwegian Sea in the North. Its average depth is about 80 m. The coastal areas are densely populated, and this fact results in extremely high human pressure over the coastal systems in the basin. Moreover, compared to the average global warming trend, the fast temperature increase recorded in the North Sea during the last decades makes the region a *hot spot* for climate change (Weinert et al., 2021).

In the entire basin, the wind-driven residual circulation is mostly counterclockwise (Mathis & Pohlmann, 2014; Quante & Colijn, 2016; Sündermann & Pohlmann, 2011) because of the prevailing Westerly and SouthWesterly winds. These wind patterns represent the mean state of the surface atmosphere flows over the North Sea because of the pressure gradient between the Icelandic Low and the Azores High acting on the region during the year and reaching its maximum in winter (Sušelj et al., 2010). Occasionally, different pressure systems generate surface

© 2023 The Authors. Earth and Space Science published by Wiley Periodicals LLC on behalf of American Geophysical Union.

This is an open access article under the terms of the [Creative Commons Attribution License](https://creativecommons.org/licenses/by/4.0/), which permits use, distribution and reproduction in any medium, provided the original work is properly cited.

**Writing – review & editing:** S. Rubinetti, V. Fofonova, E. Arnone, K. H. Wiltshire

winds from other directions, which can even reverse the mean residual transport in the basin (Stanev et al., 2019; Sündermann & Pohlmann, 2011).

Recurrent teleconnection systems, like the North Atlantic Oscillation (NAO; Hurrell & Deser, 2010), significantly affect the average wind patterns over the North Sea and are responsible for a large interannual-to-decadal variability (Feser et al., 2015; X. L. Wang et al., 2011). Their impact affects not only the mean flows over the North Sea basin but also the frequency of extreme events (Donat et al., 2010; Montreuil et al., 2016; Schmidt & von Storch, 1993; Walz et al., 2018; X. L. Wang et al., 2011).

Despite the fact that North Sea dynamics and the influence of large-scale atmospheric systems on its basin have been largely explored, an assessment of local transport in specific areas requires dedicated studies. In coastal areas, in particular, the coastline effect can significantly deviate the local wind pattern from the mean flow over the entire basin because, for instance, of the local breeze caused by the sea–land thermal gradient (Karagali et al., 2014). Moreover, wind stress exhibits variations among the sites due to their different geographical positions with respect to the location of dominant pressure centers.

The German Bight is the shallow south-eastern part of the North Sea with a maximum depth of about 50 m. Tidal amplitude ranges between about 1.5 and 3.6 m (Androsov et al., 2019). The areas with a depth of less than 20 m are well mixed due to the combination of large tidal amplitudes, complex local bathymetry, and the shape of the coastlines. Tidal residual circulation or rectification currents can be very complex, with many vortexes and locally reversed currents, so-called secondary currents (e.g., Sprong et al., 2020). However, the atmosphere also significantly controls the transport and mixing processes in the German Bight, increasing the turbulence in the surface layer and the depth of the mixed one, which in shallow areas involves the entire water column. In the case of predominant Westerly and SouthWesterly winds, an intense cyclonic (counterclockwise) pattern represents the dominant variability mode of the local circulation in the region (e.g., Callies et al., 2017; Wiltshire et al., 2010).

Despite these general characteristics, observations at several sites in the bight show that local winds exhibit significant variations in prevailing direction and intensity. To assess the changes in wind patterns in the past, present, and future, complete statistics are required, classifying wind events in terms of location, persistence, and intensity. Our study aims to implement such classification of wind events for target areas in the German Bight, analyze their seasonality and interannual variations, and explain their origin. Such effort is devoted to better understanding the dynamics of winds in one of the world's most studied and exploited basins. For instance, the wind is a crucial energy source and the number of wind farms in the North Sea, and consequently in the German Bight, has significantly improved since 1991 (Guşatu et al., 2021). Moreover, detailed knowledge of the residual sea transport caused by the wind is required to monitor and safeguard the protected areas' biodiversity.

As a base for our study, we used the ERA5 reanalysis data set, which provides homogeneous and accurate global and regional climate variables over multidecadal timescales. The Marine Protected Areas (MPAs) in the German Bight were chosen as target sites for our study because of the intensive monitoring, socioeconomic importance, and representativeness of the dynamically different sides of the region. They cover about 28% of the entire German Exclusive Economic Zone (EEZ). More specifically, we focused on the Dogger Bank, Borkum Reef Ground, and Sylter Outer Reef areas (Figure 1a). We also include in this study the Helgoland Island area because of the invaluable long-time series of measurements available at this site (Wiltshire et al., 2010). We also show how relatively close sites like the MPAs in the German Bight, in some cases, respond differently to large-scale pressure systems acting on the North Sea.

The article is structured as follows. In Section 2, the details about the data and the methods used are provided. In Section 3, the results are described, and they are summarized and discussed in Section 4.

## 2. Data and Methods

### 2.1. Reanalysis Data

Surface (10 m) horizontal wind components in the zonal (eastward)  $u$  and meridional (northward)  $v$  directions and mean sea level pressure (MSLP) data have been retrieved from the ERA5 global reanalysis data set (Hersbach et al., 2020). ERA5 is the fifth generation of atmospheric reanalysis to be produced at the European Centre for Medium-Range Weather Forecasts (ECMWF). It includes hourly estimates of the global atmosphere on a regular lat–lon grid of  $0.25^\circ \times 0.25^\circ$  ( $\sim 32$  km in the North Sea area), recently consolidated back to 1959 and constantly

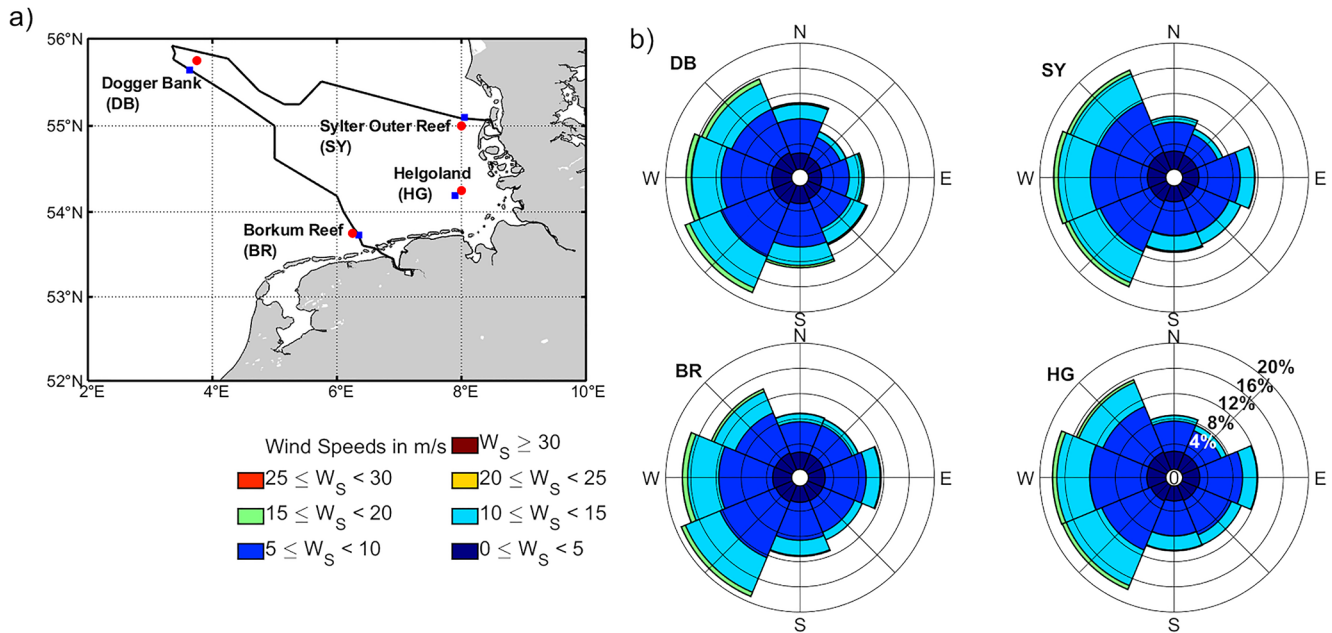


**Figure 1.** (a) German Bight (North Sea) with the four investigated sites selected for this study, namely Dogger Bank (DB), Borkum Reef Ground (BR), Helgoland Island (HG), and Sylter Outer Reef (SY). The continuous heavy black curve delimits the German Exclusive Economic Zone (EEZ; borders retrieved from Flanders Marine Institute, 2020). Red dots indicate the ERA5 grid points considered in this study, and blue squares represent the original locations of the sites. (b) Wind roses computed at the four sites are shown. The radial grid indicates the percentage of wind speed data in each direction, and the corresponding axis is shown in the bottom-right panel. The colors grouped the wind speed data according to their magnitude. The total percentages of total hours associated with each main direction are reported in Table S1 in Supporting Information S1.

updated to the current day. This allows for achieving good statistics on the wind patterns affecting the German Bight over the last decades and assessing their variability on seasonal to interannual timescales. Data are provided by the Copernicus Climate Change Service (C3S) Climate Data Store (CDS, 2023).

In this study, we considered four sites in the German Bight. Those representing the Dogger Bank, Borkum Reef Ground, and Sylter Outer Reef MPAs correspond to the extreme edges of the total extensions of the areas in the German EEZ. The Helgoland coordinates correspond to those of the Helgoland Roads time series (Wiltshire et al., 2010). The choice of these sites (blue squares in Figure 1a) is aimed to maximize the distance between the considered areas. For each of them, the time series of the 10 m wind components have been obtained by retrieving the grid points from the ERA5 data set closer to the selected sites. The grid points, hereafter DB, BR, HG, and SY, are shown in Figure 1a (red dots). Because of the resolution of the ERA5 data set, the distance between the original sites and the corresponding reanalysis grid points is about 13 km for DB, 7 km for BR, 9 km for HG, and 11 km for SY.

## 2.2. Wind Rose

Wind roses are used to visualize the most recurrent directions and magnitudes of the hourly wind data over the period 1959–2021. Eight main directions are considered resulting in sectors of 45° each. The wind roses plots are obtained with the Wind Rose MATLAB package (Pereira, 2022).

## 2.3. Self-Organizing Maps

Graphical representations of the most common MSLP pattern were obtained with the clustering algorithm based on self-organizing maps (SOMs; Kohonen, 1982, 1997). Since in this study we are dealing with not-regularly spaced pressure fields (i.e., we consider pressure fields in connection to the specific wind events) and we are not interested in preserving the variance of the signal, we preferred this approach instead of the more traditional empirical orthogonal functions (EOFs) method. The application of SOMs for geophysical pattern identifications has been increasing in recent years (Liu & Weisberg, 2011). Actually, they were more efficient in extracting

complex systems compared to the (linear) EOFs (Liu et al., 2006). Applying the SOMs method to MSLP data was already performed in previous studies: Reusch et al. (2007), for instance, used this approach to expand the knowledge about the NAO pattern beyond the current knowledge retrieved with EOFs. Furthermore, since we expect to obtain quite similar patterns—since the wind events are grouped according to the site of occurrence and direction of provenience—we consider a clustering approach more suitable for this type of study.

SOMs use artificial neural networks with unsupervised learning. Their units, or nodes, have dimensions equal to that of the input data. Each node is connected via a weighted link to each of the inputs. Before training, the weights are initialized with starting random values. The nodes are also connected to their neighbors through the neighborhood function, which determines the map's topology. The input data are presented to the network, and the activation of each node for the presented input vector is calculated using (in our case) the Euclidean distance between the node's weight vector and the input vector. The node with the lower Euclidean difference between itself and the input vector is the *winner*, and it is modified to more closely resemble the presented input vector. In addition, the neighbor nodes are updated such that each weight vector converges to the input pattern. Within the updated neighborhood, the degree of adjustment of the weights decreases away from the winning node, according to the spatiotemporal decay function or kernel. Thus, the winning node becomes similar to the input sample, and surrounding nodes develop representations of similar, but not the same, patterns. In this way, the nodes in a SOM compete to represent the particular input sample best.

During this iterative process, the rate at which the winning nodes converge to the input samples is termed the learning rate. Throughout the training, the learning rate and size of the updated neighborhood (the update radius) decrease so that the initial generalized patterns are progressively refined. After the training phase, the SOM consists of a certain number of patterns characteristic of the data, with similar patterns nearby and dissimilar patterns further apart. Further details about the algorithm can be found in Richardson et al. (2003), Liu et al. (2006), and Liu and Weisberg (2011).

In this study, we used the SOM package freely available online for MATLAB software (Vesanto et al., 1999, 2000). Several structures were implemented in this study. Here, we report the results obtained with a  $2 \times 3$  SOM array, which provides six resulting clusters. The choice of this network size allows for considering the different locations and intensities of the high- and low-pressure systems and, at the same time, summarizing the most common patterns in a limited number of clusters. The lattice structure of the network is rectangular, the initialization of node weights is linear, and the neighborhood function is the Epanechnikov one with initial and final radii of 2 and 1, respectively. The batch version of the algorithm has been chosen to improve computational efficiency. To reduce the size of the input data vector, the MSLP maps have been resampled to obtain a resolution of  $0.5^\circ\text{lon} \times 0.5^\circ\text{lat}$  (i.e., half of the original spatial resolution for both the longitude and latitude dimensions). Then, the maps were normalized according to the variance and reorganized from 2D matrices into 1D vectors. In the end, we obtained a final input matrix whose rows correspond to the time of the maximum magnitude of each event and the columns to the MSLP variables for all grid points.

### 3. Results

#### 3.1. Wind Roses of Hourly Surface Wind Data

The Dogger Bank site (DB) is the MPA farthest away from the coast: it is hence the most representative site of the open North Sea atmospheric conditions. From the wind rose of the hourly wind data at the DB site over the 1959–2021 period (Figure 1b), it is clear that the dominant pattern is represented by SouthWesterly winds, whose intensity is higher during the December–January period (see Figure S1 in Supporting Information S1 for the month-by-month analysis). This atmospheric flow, together with the Westerly winds, represents the most common mean state of the atmospheric system over the entire North Sea during the year, as also demonstrated by the monthly values averaged over the total period 1959–2021 over the North Sea region (Figure S2 in Supporting Information S1). A slightly lower percentage of occurrences is represented by the NorthWesterly winds, whose occurrence is relevant in particular between April and July (see Figure S1a in Supporting Information S1), while low frequency is associated with winds from the East. Their occurrence is largely limited to the spring season, as will be discussed in the next sections. Note that Easterly winds are more frequent at the coastal sites (BR, HG, and SY) compared to the DB one (Figure 1b; Figure S1 and Table S1 in Supporting Information S1). Finally, the Sylt Outer Reef (SY) site deviates from all the others for the percentage of winds blowing from North-West with a remarkable dominance over the other directions from April to August (Figure S1d in Supporting Information S1).



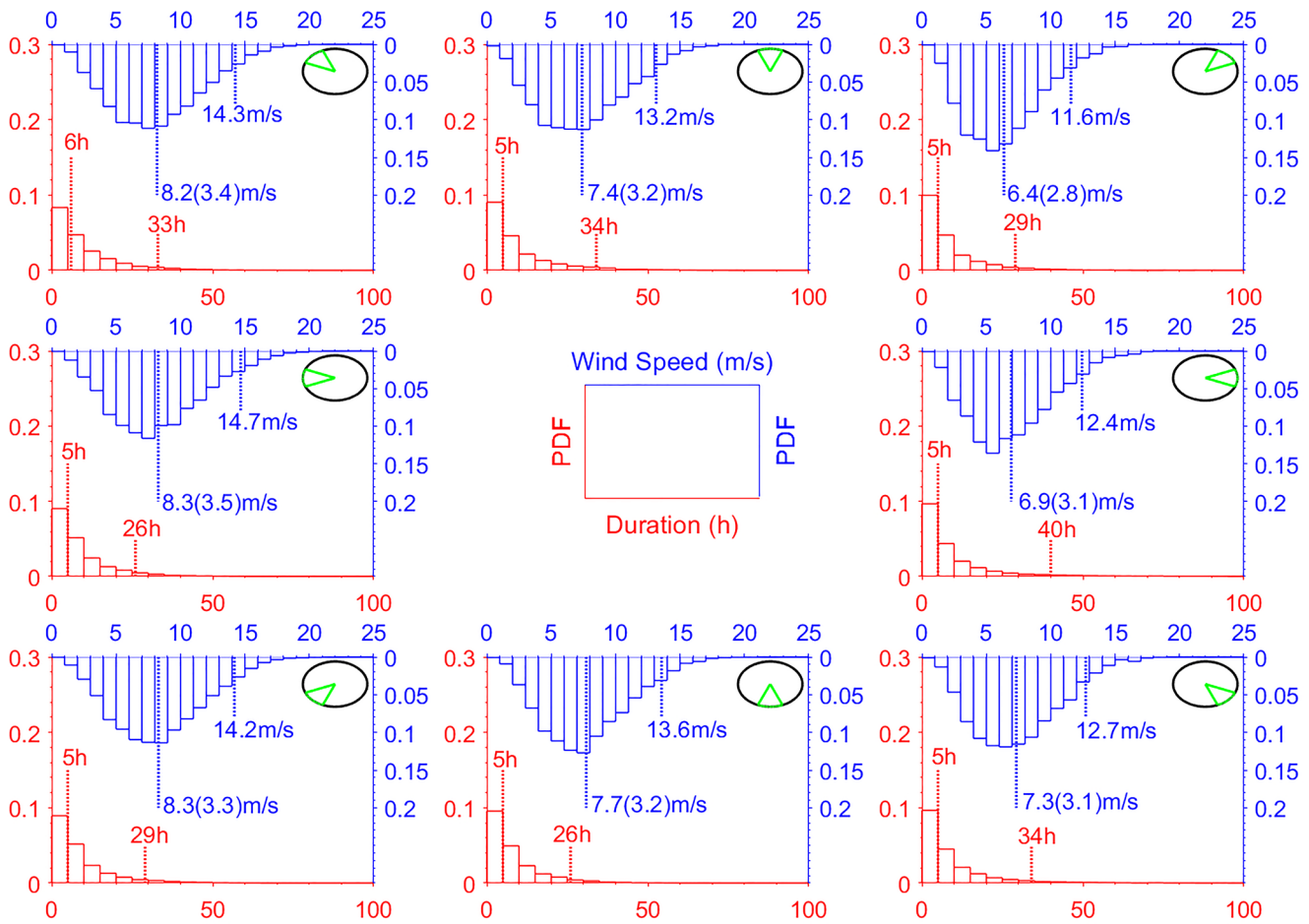


**Figure 2.** Summary of statistics of wind segments according to the main direction (green sector on the top right). In each panel, the red histogram shows the distribution of the duration of all events (i.e., subsequent hours with the wind from the same direction). Dotted red lines indicate the median and the 95 percentile values. The blue histogram represents the distribution of the average wind speed of each segment (after having discarded those too short). The dotted blue lines report the values of the distribution's mean (with the standard deviation reported in parentheses) and the 95 percentile. The central panel reports the axis labels. Distributions refer to the Dogger Bank (DB) site (see also Figure S3 in Supporting Information S1 for the other sites).

Wind roses provide a useful inspection of the distributions of hourly wind data according to their magnitude and direction. To define wind events in terms of persistence and average speed, grouping subsequent hours in the same direction is necessary. This is the topic of the following subsection.

### 3.2. Wind Event Selection

Considering consequent hours with the wind blowing from the same main direction as a unique *segment*, the distributions of the duration ( $D$ , in hours) of the surface atmospheric flows have been obtained for each site. Eight main directions are considered in this study (hereafter E, NE, N, NW, W, SW, S, and SE), as already shown for the wind rose computations.

The statistical analysis of the duration returns highly asymmetric distributions with the maximum corresponding to 5 or 6 hr. It is clearly visible in Figure 2 (red histograms), which shows the results for the DB site (see Figure S3 in Supporting Information S1 for the other locations). The numbers reported in red indicate the median of the distribution and the 95 percentile. Comparing the results among the different directions, it can be noticed that while the median values are overall equal (taking into account 1 hr time resolution of the data set), relevant differences are detectable at the right edges of the distributions, with a remarkably high value of  $D$  for the Easterly winds. By reporting in the same plot the values of the median (Figure 3a) and the 95 percentile (Figure 3b), it can be observed that the first is quite homogeneous among all sites and directions with an average value of 5 hr.

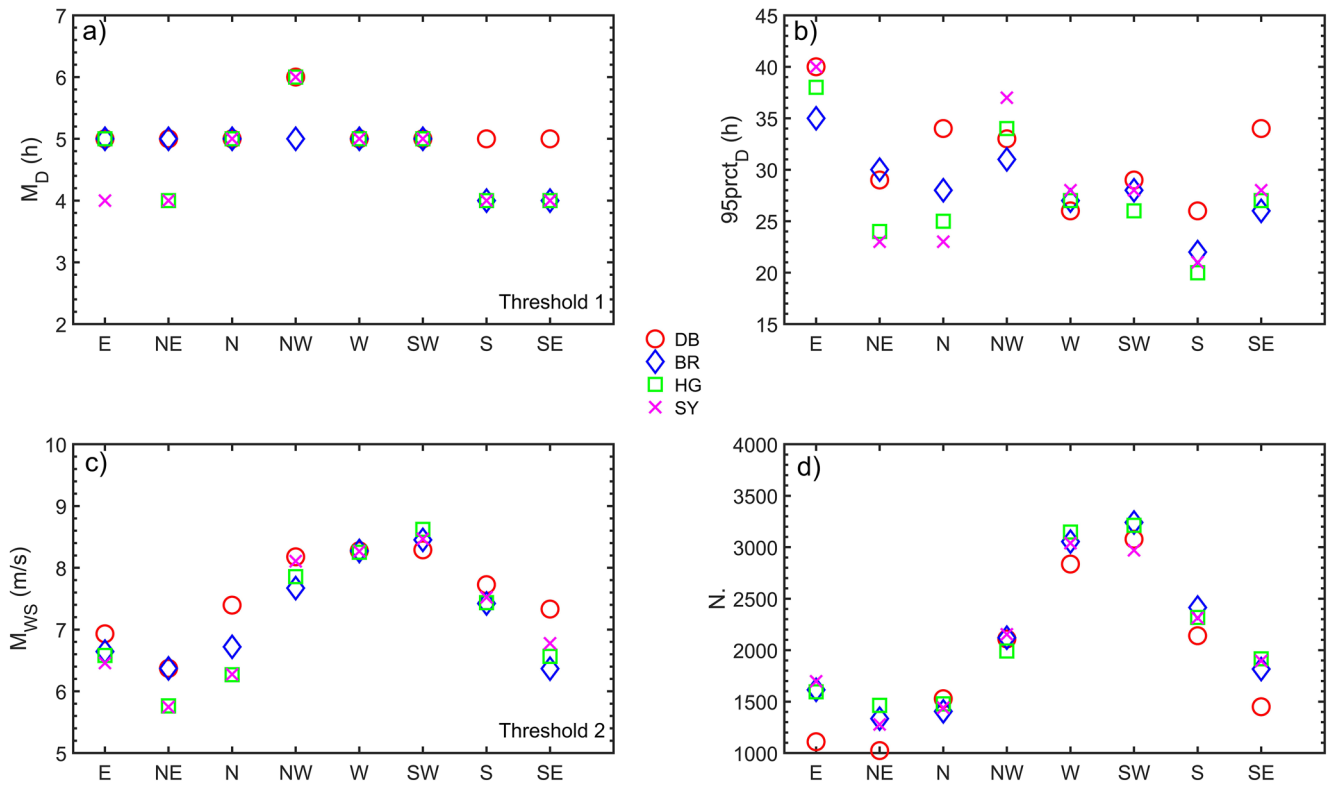


**Figure 3.** Summary of basic statistics of wind events, including median ( $M_{D}$ , a) and extreme duration ( $95prct_{D}$ , b), mean wind speed ( $M_{WS}$ , c), and the resulting number of events (d), that is, segments when the surface wind has had the same main direction for at least a number of hours equal to the median duration (shown in panel a as threshold 1) and whose mean speed is equal at least to the mean of the distribution (panel c as threshold 2).

On the contrary, relevant differences are detected for the extreme durations: E winds are those that can persist for longer periods; for instance, the longest event at SY started on 22 May 1992 and lasted about 11.7 days, with an average wind speed of 7.8 m/s. NW winds also show high values at the edges of the distributions, particularly at the SY site. In fact, the longest event present in the entire data set started on 15 July 1984 and lasted 295 hr (12.3 days), with an average wind speed of 9.3 m/s. However, this is an exceptional case of such a long persistence of an NW wind event (the second longest lasted *only* 152 hr). On the contrary, the duration distributions of E winds present a higher uniformity at the edges (i.e., several events have similar long durations at the edge of the distribution).

As a result of this analysis, a remarkable number of segments persisted for a short time interval. Discarding such short segments is crucial for providing a reliable estimate of the average magnitude of the wind patterns (computed over a significant number of hours) and retrieving only those cases which can effectively play a role in the dynamics of the considered areas. Therefore, considering the strong asymmetry of the duration distributions, the median of  $D$  ( $M_{D}$ ) is chosen as the suitable threshold for discarding all those segments shorter than  $M_{D}$ . The values are reported in Table 1.

Successively, the magnitude of the wind events is obtained by averaging the wind speed over the entire duration of the remaining segments. Thus, the distributions of average wind speeds are obtained and shown in Figure 2 (blue histograms). In the figure, the vertical blue lines indicate the mean of the distribution  $M_{WS}$  (with standard deviation in parentheses) and the 95 percentile. In contrast to the duration distributions, the average speed ones return a more symmetric shape around the mean value, with, in all cases, a positive skewness. The direction with the lowest mean speed is represented by NE winds (5.7 m/s), while W and SW winds have the highest mean intensities ( $\sim 8$  m/s). All distributions present comparable values of the standard deviations (about 3 m/s). W winds return the highest value of the edge of the distribution (14.7 m/s). We remark that the average speed distributions have been obtained after discarding the segments with duration shorter than the median  $M_{D}$ . In this study, we estimate the  $M_{WS}$  values by computing the arithmetic mean. An alternative approach could be fitting

**Table 1**  
*Summary of Statistics of Wind Events in the German Bight*

	E	NE	N	NW	W	SW	S	SE
Duration								
DB	5 (40)	5 (29)	5 (34)	6 (33)	5 (26)	5 (29)	5 (26)	5 (34)
BR	5 (35)	5 (30)	5 (28)	5 (31)	5 (27)	5 (28)	4 (22)	4 (26)
HG	5 (38)	4 (24)	5 (25)	6 (34)	5 (27)	5 (26)	4 (20)	4 (27)
SY	4 (40)	4 (23)	5 (23)	6 (37)	5 (28)	5 (28)	4 (21)	4 (28)
Average wind speed								
DB	6.9 (12.4)	6.4 (11.6)	7.4 (15.1)	8.2 (14.2)	8.3 (14.7)	8.3 (14.2)	7.7 (13.5)	7.3 (12.7)
BR	6.6 (11.1)	6.4 (10.9)	6.7 (11.6)	7.7 (13.4)	8.3 (14.2)	8.4 (14.0)	7.4 (12.7)	6.4 (10.9)
HG	6.6 (11.1)	5.8 (10.4)	6.3 (10.6)	7.9 (13.3)	8.3 (13.9)	8.6 (13.9)	7.4 (12.7)	6.6 (11.1)
SY	6.5 (11.2)	5.7 (10.5)	6.3 (10.9)	8.1 (13.6)	8.3 (13.9)	8.5 (14.1)	7.5 (13)	6.8 (11.5)
Number of events/year								
DB	74	70	95	137	177	186	142	95
BR	101	90	94	131	182	195	143	107
HG	104	96	99	134	185	190	141	110
SY	98	91	102	137	180	183	139	108

*Note.* Top: median duration ( $Md_D$ , in hours) of the wind segments from each main direction shown in Figure 2 (red histograms). The 95 percentile ( $95prct_D$ , in hours) of the event durations are reported in parentheses. Middle: mean wind speed ( $M_{WS}$ , m/s) in each main direction for events lasting at least as their medians from the distributions shown in Figure 2 (blue histograms). In parentheses, the 95 percentile is shown. Bottom: the average number of events per year (over 63 years period) resulted from discarding the segments too short (threshold 1) and then those with an intensity lower than the mean (threshold 2). The values are summarized in Figure 3.

the distribution with a theoretical one, like the three-parameter Weibull distribution, which is widely applied to wind speed data (see, e.g., Z. Wang & Liu, 2021) and then retrieve the mean as a first moment. In our case, the bias between these two approaches would be less than 1% in all cases.

Again, to have an overall picture of the mean wind speed among all sites and directions, we can look at Figure 3c and Table 1. W and SW winds correspond to the highest values of  $M_{WS}$  (~8.5 m/s), with comparable values among all sites. NW winds are also characterized by high values of mean wind speed, especially at the northernmost sites (DB and SY). The DB site is almost always associated with higher values of the magnitude of the winds from all directions, compared to the other sites, probably because of its location in the open sea. Winds from NE are, on average, the less intense ones (~6 m/s) over the German Bight.

To properly select only the most intense events,  $M_{WS}$  is applied as the second criterium to discard the segments whose average speed is lower than this threshold. The total number of the retrieved segments, grouped according to the site and directions, is shown in Figure 3d and represents the resulting catalog of *wind events*. To summarize, this catalog of wind events results from a twofold selection based on the typical duration and intensity of the wind segments over the 1959–2021 period. This procedure is crucial to obtain a data set whose persistence and intensity significantly deviate from the calm atmospheric state. The average annual frequency of the wind events (see Table 1) ranges from 70 events/year for E wind events to 195 events/year for SW wind events. As expected, the W and SW winds are the most frequent patterns with the highest mean speed values for all considered sites. S winds are more frequent than NW ones; nevertheless, the latter pattern generally has a higher intensity. N, NE, and SE winds are the lowest frequencies and intensities patterns. As reported before, E winds, besides the reduced number of events compared to the other directions, have the highest value of extreme duration. The number of events is comparable at all sites for each main direction. The most relevant differences are the lowest number of SE, E, and NE events at the DB site compared to the other areas.

At this point, it is necessary to assess the effects of the applied thresholds, that is, to quantify the number of hours and the amount of energy discarded because of them. The duration threshold causes the removal of 12% of the total number of hours in the data set, and this percentage is the same at all sites. The second threshold, based on

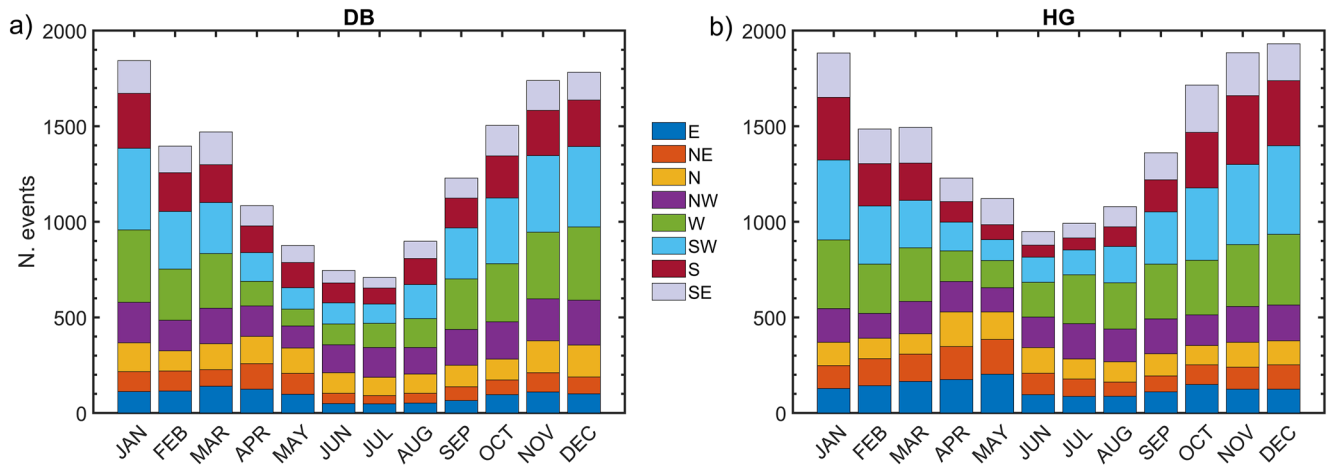


**Figure 4.** Seasonality of selected wind events according to the month of occurrence and direction. The results refer to the Dogger Bank (DB; left) and Helgoland Island (HG; right) sites.

wind speed, results in a total rejection of about 48% at HG, 48% at SY, 49% at BR, and 51% at DB of the total hours. It is clear from this result that the second threshold is crucial, especially at the DB site, which is located in the open sea and then returns higher velocities for most of the directions compared to the other coastal sites (see Figure 3c). In addition, we use the kinetic energy per unit of mass ( $E_k = \frac{1}{2}V^2$ , where  $V = \sqrt{u^2 + v^2}$ ) to estimate the amount of energy of the surface wind. Hence, by integrating  $E_k$  over the entire time period of ERA5 data set at each point (regardless of the direction), we obtain the total amount of energy. Then, by computing the same quantity over the retrieved segments (again, regardless of the direction), the percentage discarded by applying the threshold is obtained. Because of the first threshold, about 7% of the total energy is lost at all sites. The total percentage of energy which is discarded by applying both thresholds is 24% for the coastal sites and 25% for the DB one, thus confirming how significant is the application of a threshold based on the magnitude of the wind. Obviously, there are numerous possibilities regarding the choice of the duration and speed thresholds. By increasing the desired duration of the wind events (threshold 1), and still using the average wind speed from the retained segments as threshold 2, could lead to a maximum of about 77% of total energy loss and 87% of total hours discarded. By keeping the median of duration as threshold 1, but increasing the desired wind intensity (threshold 2), we could reach a rejection of about 90% of the total energy and even 97% of total hour discarded (see Figure S4 in Supporting Information S1). The resulting number of events would, of course, be affected by the choice of these parameters, even if the distribution of the events among the different directions would be the same, with prevailing SW and W winds. Only when extreme wind intensities are considered (i.e., those values beyond the 2-standard-deviation range in this case), the frequency of the winds from all directions, except for SW and W winds, is comparable (see Figure S5 in Supporting Information S1).

### 3.3. Seasonality of Wind Events

The threshold applied to select the events results in a clear seasonal behavior of not only the most frequent direction in different periods of the year but also (and especially) the total number of events. This fact is clearly visible in Figure 4a for the DB site. The total number of events grouped according to their month of occurrence shows a clear minimum in June and July and a maximum in November–January. All wind patterns from W to SW show a clear predominance during the autumn and winter seasons. Winds from E and NE have a larger occurrence during spring. One of the most evident differences is that the HG site shows many Easterly wind events during May, not recorded elsewhere (Figure 4b).

While the persistence of winds from a certain direction does not return a clear seasonal behavior (not shown), the magnitude shows an intense annual modulation. If we consider the average speed distribution like those in Figure 2 (blue histogram) but obtained after having grouped the segments according to their month of occurrence (i.e., for each site and main directions, 12 wind speed distributions are obtained instead of only one), we get the values shown in Figure 5. All the minima of the mean speed are reached between May and August. On the



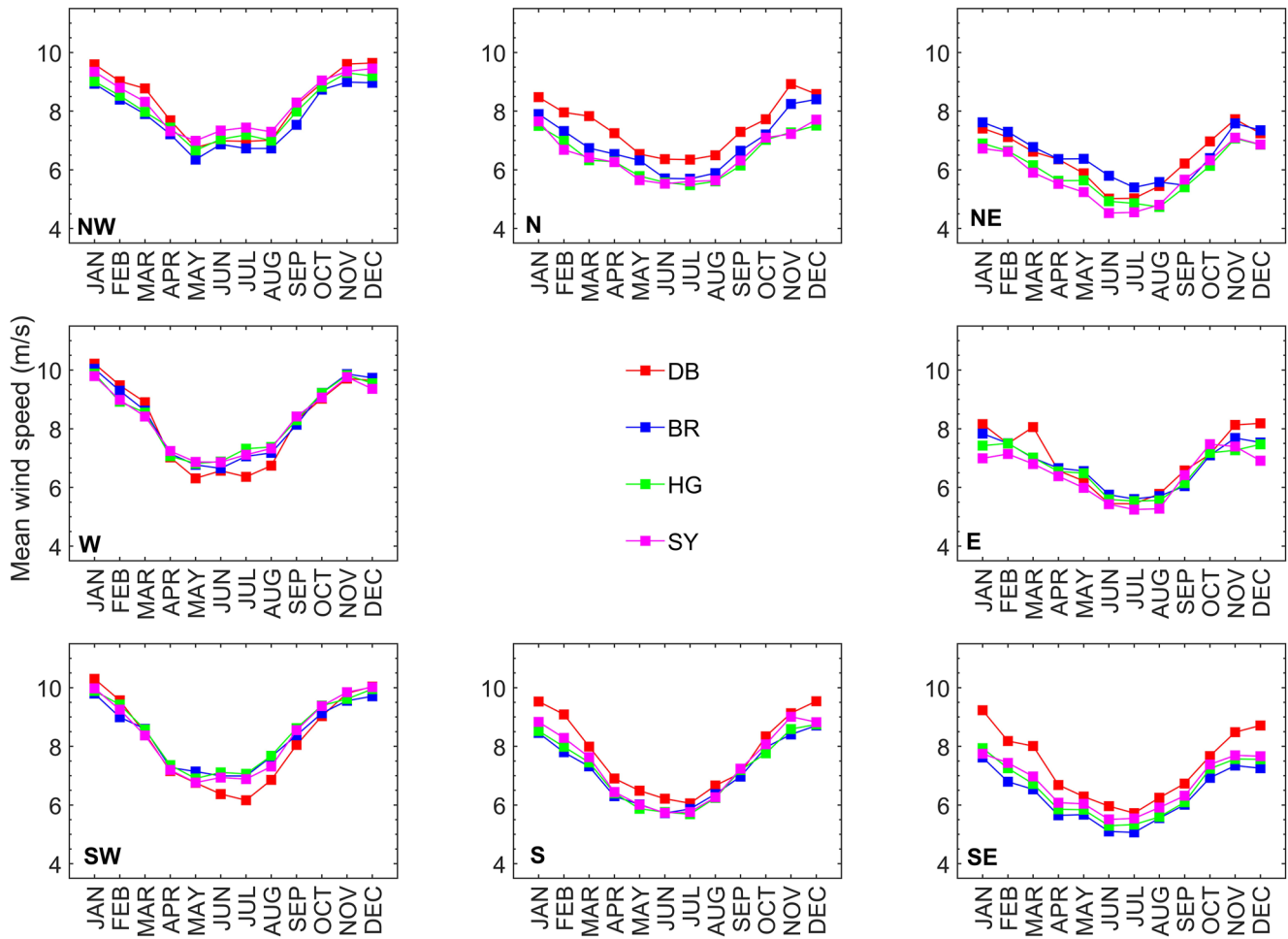


**Figure 5.** Seasonality of the mean value of the average wind speed grouped according to the site and the main direction (indicated by the green sector on the top of each panel). Colored curves indicate the mean of the distributions of the average wind speed of the segments lasting at least as  $Md_p$  (shown in Figure 3a).

contrary, the maxima occur mostly between November and January. The annual cycles for each direction are quite the same at all sites. The higher values during winter are mostly the result of the strengthening of the pressure gradients during the winter season, causing an intensification of the surface flows over the North Sea basin. This fact emerges from the analyses of the MSLP maps reported in the following subsection.

### 3.4. Large-Scale Pressure Patterns and Their Effects on Local Winds

In this study, we provide a data set of wind events at four specific sites in the German Bight (Figure 3 and Table 1). They are mostly the result of large-scale pressure lows and highs over the North Atlantic and Europe, with their location and intensity significantly affecting the features of the local flows. A wind event can result from a specific configuration of the pressure fields: therefore, classifying the most common pressure patterns can aid in interpreting our wind statistics. For this reason, we apply a clustering approach to distinguish different possibilities regarding MSLP values.

For each wind event, the MSLP map over the entire North Sea basin has been extracted from the ERA5 hourly resolution pressure data (CDS, 2023). The timing of each map corresponds to the hour when the highest wind speed of the considered segment has been recorded, which, at first order, is directly related to the strongest pressure gradient. Therefore, considering, for example, the SW winds at the DB site, we obtain 3,078 events over the 1959–2021 period (Figure 3d). Consequently, we retrieve 3,078 MSLP maps for such wind patterns at this site. We use the SOMs method to provide six different pressure patterns for each main direction of the local winds and each site. Considering the large number of cases, only a few examples are shown in the text. All the results are, however, included in Supporting Information S1 (Figure S6).

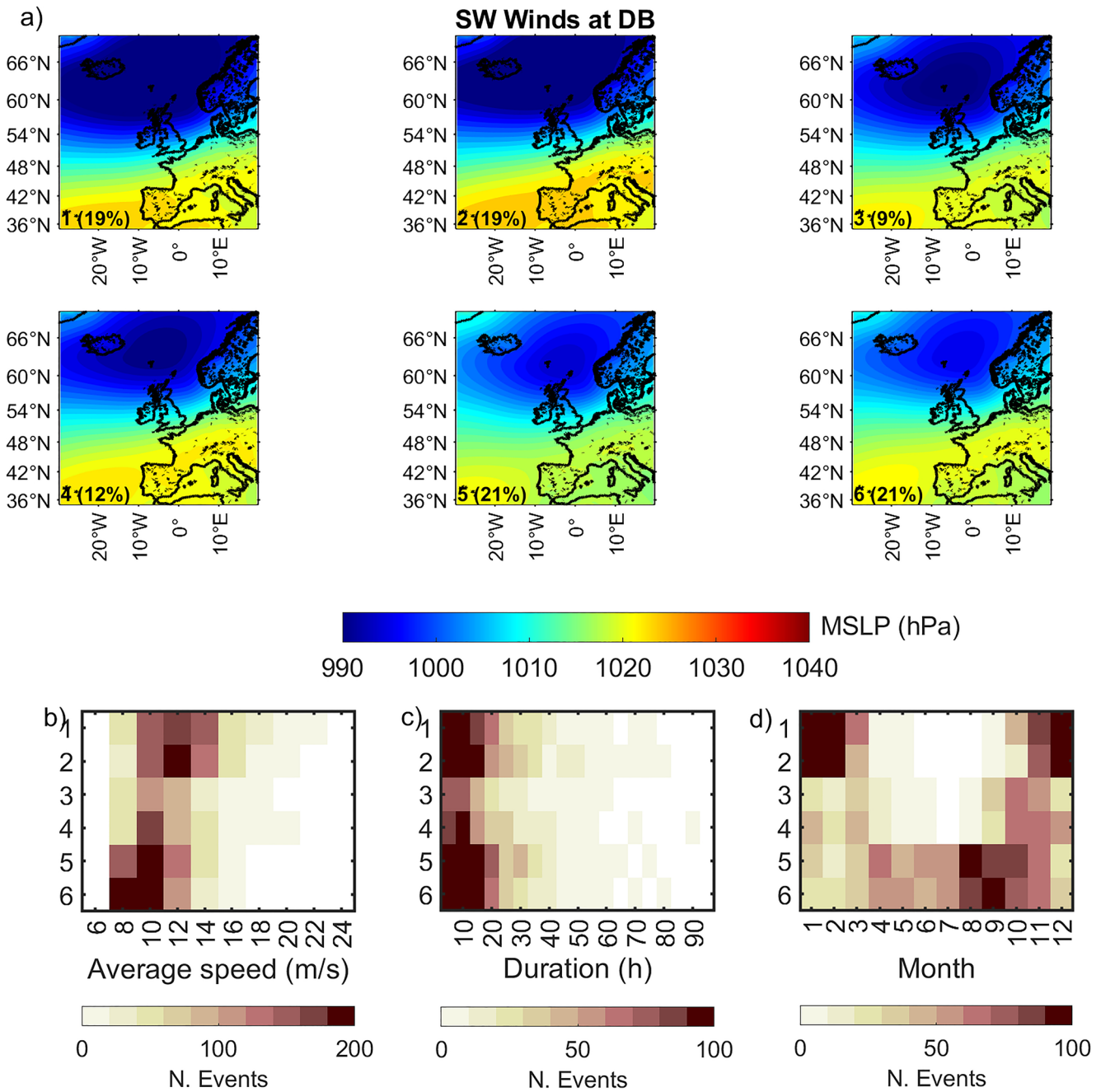


**Figure 6.** Features of the mean sea level pressure (MSLP) patterns causing the SW winds at the Dogger Bank (DB) site. (a) MSLP patterns from the self-organizing maps (SOMs) clustering analysis. Numbers at the bottom left indicate the cluster number and the percentage of the total original pressure maps associated with it (in parentheses). (b) The average wind speed distributions for the events caused by each of the six clusters. (c) The duration distributions. (d) Distribution of event numbers through different months for each considered cluster.

Starting from the SW at the DB site, the resulting clusters are shown in Figure 6a. It clearly emerges from the pressure maps that the dominant feature is the pressure minimum located North of the British Isles, with several possibilities concerning its extension. We start from the strong pressure difference between the depression over the North Atlantic and the high-pressure system covering the whole of continental Europe shown by cluster 1 to the case of the localized pressure minimum of cluster 6. Each cluster is the most representative of a certain number of the original MSLP maps, and this percentage is reported in parentheses. For instance, 19% of the total 3,078 SW wind events at the DB site have been generated by a pressure system shown in cluster 1. In panel b, the

distributions of the average wind speed are reported. In this case, the events are grouped according to the associated cluster (y-axis). Therefore, we can see that while cluster 1 causes surface winds with a speed distribution with a large peak between 9 and 15 m/s, clusters 5 and 6 correspond to the lowest average speed (between 7 and 11 m/s). Cluster 1 originates the flows with the highest mean wind velocities and also the most positive skewness. In panel c, the distributions of the duration of the events are shown, and the positive skewness is evident by looking at the values corresponding to durations longer than 60 hr. In any case, the peaks of the distributions always correspond to quite short durations, as expected from Figure 2. Finally, the distributions of the seasonality of the different pressure patterns are shown in panel d. Localized dipole with the low minimum over the Northern British Isles and the high pressure over the Azores is more frequent during the spring and summer period, between March and September (clusters 5 and 6). The winter systems are characterized mainly by extended low pressures between Iceland and the Scandinavian peninsula and high-pressure values over the Azores and Western Europe.

Regarding the similarities between the different sites, while the winter patterns have almost the same effect over the entire German Bight during the spring and the summer periods, the pressure minima over the northern part of the UK are more effective at the DB site. When the cyclonic structure moves eastward, it causes the SW flows over the other sites (Figures S6.14, S6.22, and S6.30 in Supporting Information S1).

Similarly, blocking systems over the British Isles and North Sea basin generate S winds instead (see Figures S6.7, S6.15, S6.23, and S6.31 in Supporting Information S1). The most relevant feature of such systems is that they only partially cover the North Sea basin, thus causing a geostrophic flow from South to North. Also, in this case, localized cyclonic systems are more frequent during the spring and summer seasons.

Analogous results are obtained for the W winds: a clear seasonality is obtained, linked to the strength of the high- and low-pressure centers, and the pressure systems' features are comparable with respect to the SW winds. The localized cyclonic systems acting during spring and summer are, in this case, shifted eastward over the Scandinavian peninsula (see Figures S6.5, S6.13, S6.21, and S6.29 in Supporting Information S1).

Regarding the NW winds (Figure 7 and Figures S6.4, S6.12, S6.20, and S6.28 in Supporting Information S1), in most cases, the dominant feature is the anticyclonic system over the Azores or the Celtic Sea. The minimum is shifted toward the southern part of the Scandinavian peninsula. Localized high-pressure centers over the Celtic Sea (e.g., clusters 5–7) are more frequent between April and August. As in the previous cases, the patterns more recurrent during the winter season correspond to the highest mean wind speed (cluster 2). With respect to the SW and W winds, the tale of the distributions of persistence of the NW winds is shifted toward higher values, especially at the SY site. It is interesting to note that the pressure patterns with the highest probability of long persistence (>50 hr; clusters 5 and 6) occur mostly in the spring or summer seasons.

When the anticyclonic system moves over the British Isles, N winds persist in the entire German Bight (Figures S6.3, S6.11, S6.19, and S6.27 in Supporting Information S1). When a high-pressure center forms the pressure dipole between the British Isles and southern Scandinavia and the low one over continental Europe, NE (Figures S6.2, S6.10, S6.18, and S6.26 in Supporting Information S1) and E winds are formed. The second pattern (Figure 8 and Figures S6.1, S6.9, S6.17, and S6.25 in Supporting Information S1) is particularly interesting because of its higher probability of occurrence. We previously showed that at the HG site, the highest number of such events had been recorded, with a peculiar frequency peak during May. In Figure 8d, it is shown that this is due to an intense anticyclonic system over Scandinavia associated with a less pronounced pressure minimum over Europe (clusters 1, 2, and 5).

While the low-pressure center moves over the Northern North Sea basin and the high pressure strengthens over Western Europe, SE winds are generated (Figures S6.8, S6.16, S6.24, and S6.32 in Supporting Information S1) and then S ones. Ultimately, the region returns to the patterns causing the S and SW winds.

### 3.5. Interannual-To-Decadal-Scale Variability of Wind Patterns

The interannual and decadal variability of wind events (especially the most intense ones) in the North Sea is one of the most debated topics. On the one hand, the ability of regional models to predict the frequency and variability of such events is crucial for safeguarding human activities and exploiting natural resources in coastal areas. On the other hand, a clear relationship between such events and large-scale teleconnection would allow the insertion of local variability into climate change context.

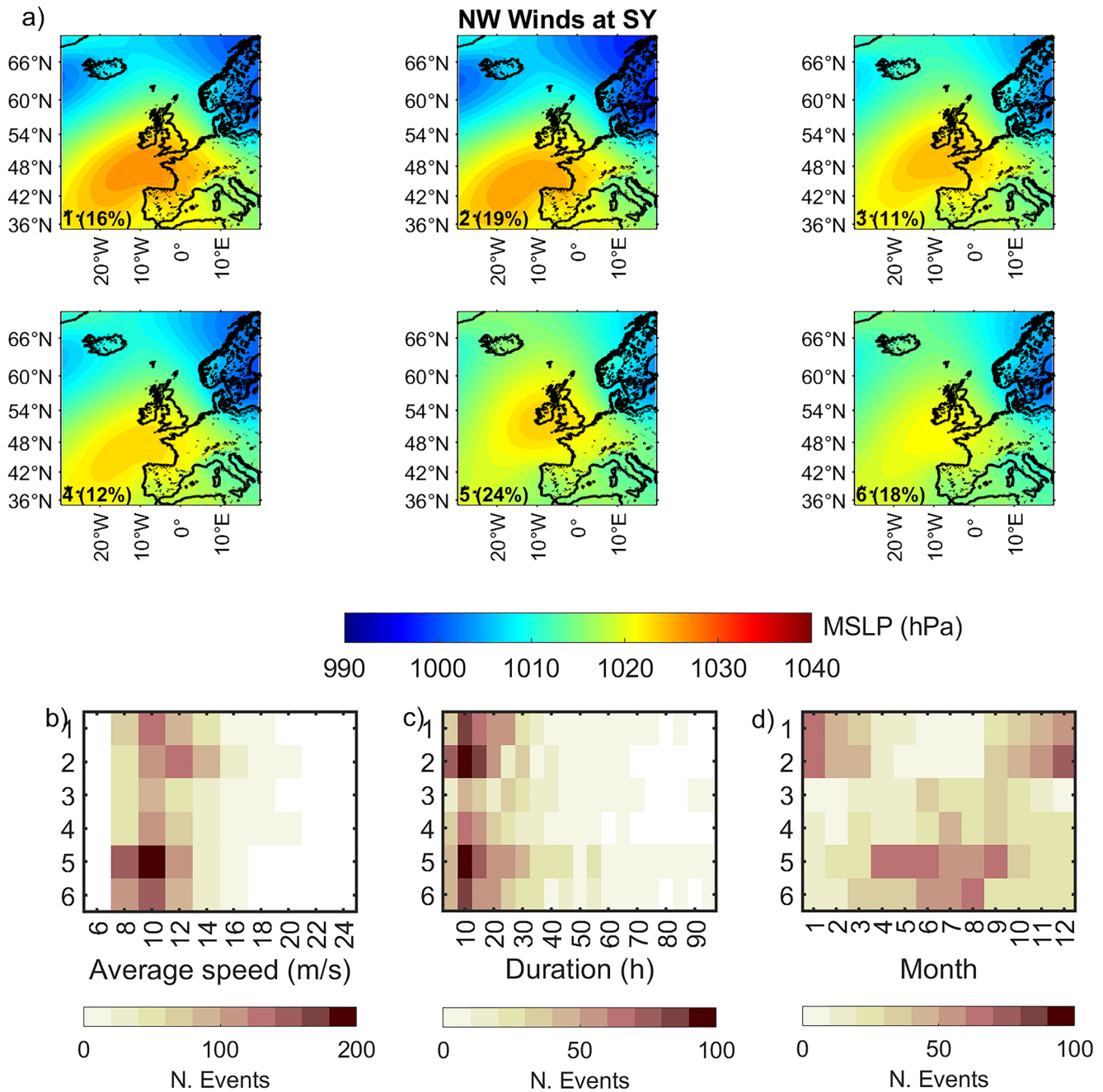


**Figure 7.** Same as Figure 6 for NW wind events at the Sylter Outer Reef (SY) site.

Annual frequency exhibits variation within different directions and sites (Figure 9). W and SW winds show a high correlation between the time series at the different sites. On the contrary, winds from E, NE, N, and SE return higher discrepancy (see also Figure S7 in Supporting Information S1). In particular, the DB site shows significantly different responses to those patterns, demonstrating that they mostly originated from the coastline effects on the mean flow over the North Sea basin.

Only the SW and S winds return significant ( $p$ -value  $< 0.05$ ) increasing linear trends over the entire period of the annual time series, equal to about  $+0.18$  events/year in the case of SW and  $0.13$  events/year for the S winds.

Concerning the interannual variability, in some cases, peculiar years with significant low or high frequencies of the events are detectable. For example, E winds show a prolonged minimum around 1990, while SW and W



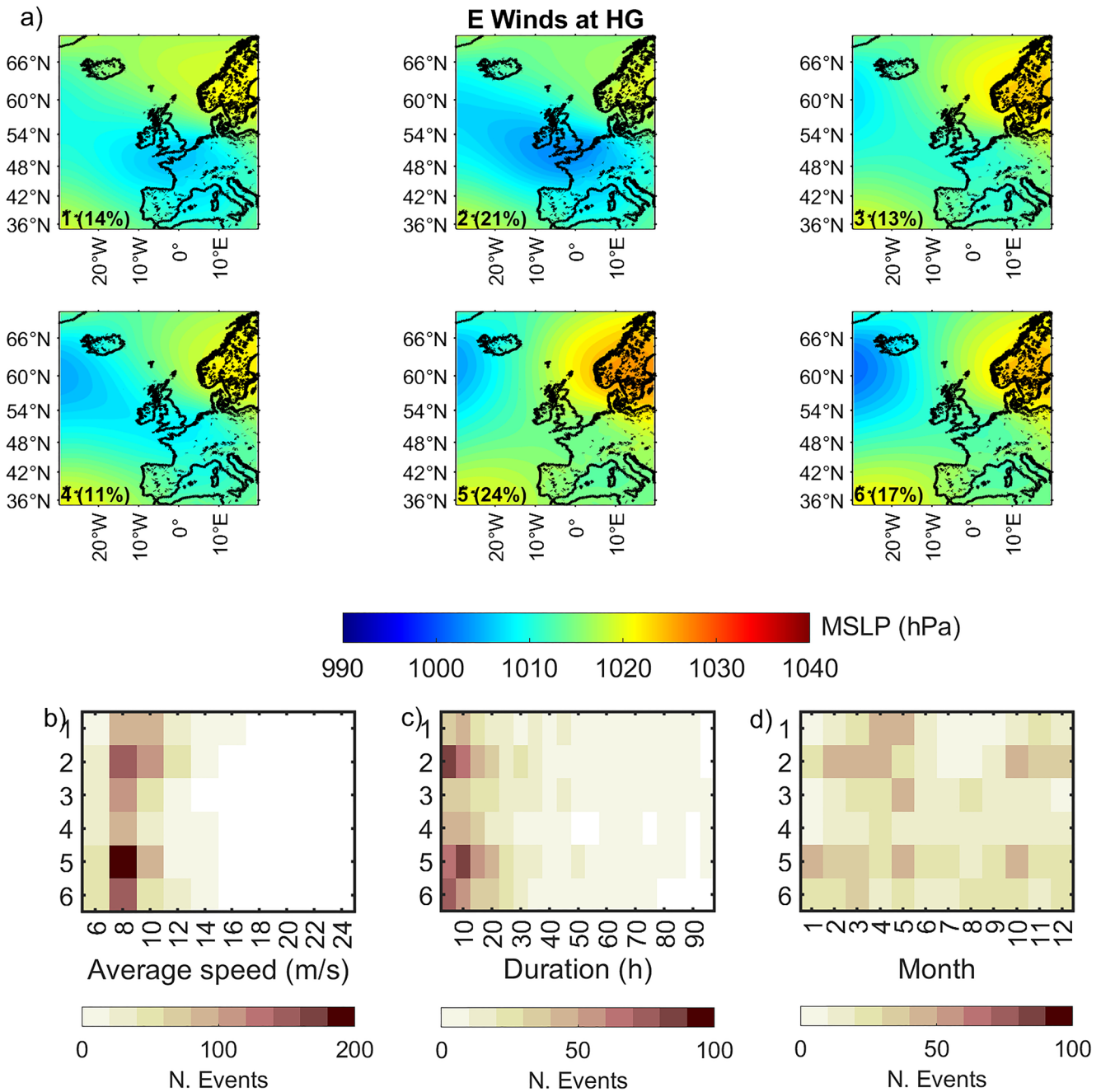


**Figure 8.** Same as Figure 6 for E wind events at the Helgoland Island (HG) site.

winds have low frequencies in 1996 and 2010. S winds return a significant maximum in 2000 and increased the frequency of events in the last decades (about 1 event/year).

#### 4. Discussion and Conclusions

This study is dedicated to analyzing wind patterns characterizing the local variability in the MPAs in the German Bight (North Sea). Here, we define *wind events* as subsequent hours with the wind flowing from the same direction with a duration and intensity higher than specific thresholds. We provide this definition for four selected sites, namely the MPAs in the German EEZ and the Helgoland Island. The results are based on the statistical analysis of hourly surface wind speed and directions retrieved from the ERA5 reanalysis data. To the best of

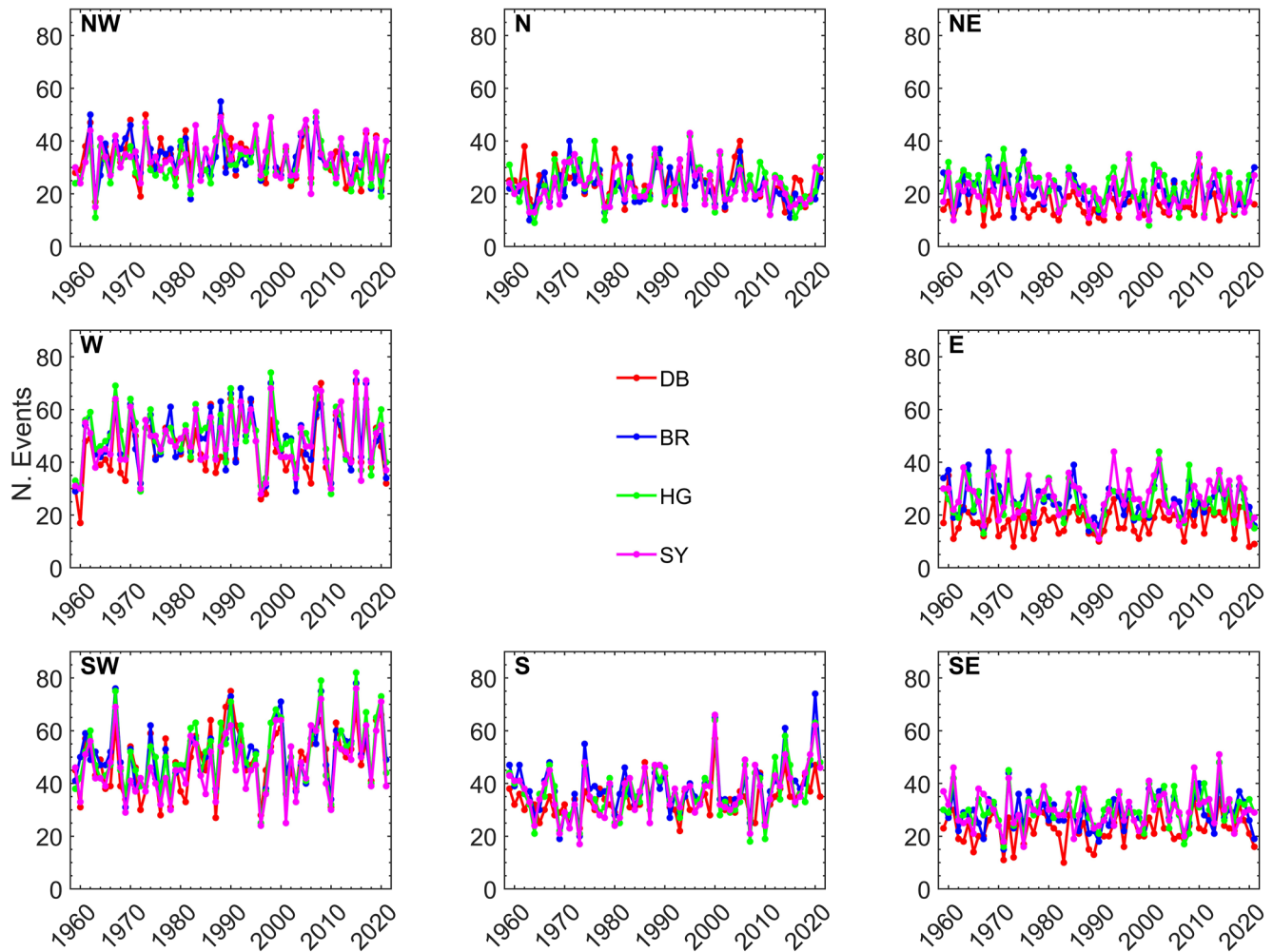


**Figure 9.** The number of events per year corresponding to each wind pattern and recorded at each site.

our knowledge, this is the first study assessing the local features of wind events in the German Bight. Using the reanalysis data instead of local measurements allows for comparing the results among the selected sites.

We show that the mean state is represented by SW and W winds, as already demonstrated by previous studies. Similar results for the entire southeastern portion of the North Sea have been obtained for the 1971–2000 period (Bülow et al., 2013; Quante & Colijn, 2016). Bülow et al. (2013) compared the wind data from the ERA40 reanalysis data set with outputs from regional climate models over the 30 years 1971–2000, driven by boundary conditions of the reanalysis ERA-40. One of the results is that some regional models show a predominance of the Westerly winds with respect to the SW ones, in disagreement with the reanalysis data (see also Ganske et al., 2016). Concerning the wind speed, also in our case, we can expect an underestimation of the intensity due to the limited resolution of the reanalysis data (Kalverla et al., 2019, 2020).

As expected, whereas the selected sites are quite close to each other, several differences are detectable: in particular, the Dogger Bank area, located farthest away from the coast, is less affected by winds from the East with respect to the other regions. In the meantime, the Sylt Outer Reef MPA is the most exposed to winds from North-West.

The intensity of SW and W winds is higher during the autumn–winter seasons. The highest average wind speeds also characterize them. S and NW winds are the other relevant patterns because of their intensity and frequency. E winds are not frequent in the German Bight, but they can persist for several days when they occur. Intense winds show a clear seasonal pattern, with a minimum speed during the summer period and a maximum in October and

January. This seasonal cycle is linked to the strength of the pressure systems acting on the region, whose gradients are particularly large during the fall and winter seasons.

Different pressure systems can originate the same wind pattern over a specific area. The SW and W winds are caused by the westerly flows over Northern Europe originating by the large-scale pressure gradient between the Icelandic Low and the Azores High, whose extension and strength reach their maximum in the winter season. In addition, also localized cyclonic systems over the British Isles can generate such winds. Looking at the MSLP maps resulting from the clustering analysis, it is clearly evident that most of them resemble the typical features of the NAO. In fact, the interannual variability of wind events is partly related to the large-scale modes. Among them, the NAO is the most important and discussed one. By definition, it is strictly related to the strength of the westerlies and the eddy-driven jet stream over the North Atlantic and Western Europe (Hurrell & Deser, 2010). Several studies aimed to find a direct linkage between the NAO and the ocean dynamics in the North Sea (Callies et al., 2017; Mathis et al., 2015) and storm frequency (Donat et al., 2010; Siegmund & Schrum, 2001; X. L. Wang et al., 2011). Such teleconnection systems affect the mean surface flow over the North Sea basin, while local effects also influence the selected sites. Nevertheless, a clear impact of NAO on the German Bight is visible during the years with the lowest frequency of W and SW winds (e.g., 1960, 1996, and 2010), which correspond to extremely low phases of the NAO index. On the contrary, the high values in recent years (e.g., 2015, 2017) coincide with its current prolonged positive phase. The positive NAO phase can also partly explain the high number of S wind events in 2000 and their positive increase in recent decades. The number and average speed of wind events, especially from W and SW, are higher during winter. Nevertheless, during some periods, we detect higher frequencies of wind events and an increase in their intensity and a shift of their peaks from December/January to February/March during the end of the 1980s and the early 1990s (see Figures S8 and S9 in Supporting Information S1). This result has been previously obtained by Siegmund and Schrum (2001), who analyzed the wind speed over the entire North Sea using the NCEP reanalysis data. However, this shift toward late winter/early spring is particularly evident only in these years: no similar cases (with comparable frequency and intensity of the winds) are detected in the recent decades.

Whereas the NAO has been widely recognized as the dominant large-scale teleconnection system affecting the atmospheric variability over the North Sea, several other patterns, resulting from being highly significant modes of the SLP over the North Atlantic, must be taken into account (Barnston & Livezey, 1987; Walz et al., 2018). Mailier et al. (2006) and Walz et al. (2018) identified five teleconnections linked to pressure systems in the Northern Hemisphere impacting interannual variability of cyclone system number over Europe, namely the NAO, the Eastern Atlantic (EA), the Scandinavian (SCA), the Eastern Atlantic/Western Russia (EA/WR), and the Polar (POL) patterns. Walz et al. (2018) also include the Northern Hemisphere ice cover as a significant driver in the previous list because of the temperature gradient variability between the polar region and the European continent. Among all of them, the Scandinavian one (SCA) has been recognized as one of the most important ones in Northern Europe (Barriopedro et al., 2006; Quante & Colijn, 2016) and the southern part of the North Sea (Walz et al., 2018). In its positive phase, the occurrence of high-pressure systems over the Scandinavian regions increases. Therefore, its significantly negative phase around 1990 could explain the local minimum of E winds in that period.

It is worth considering that teleconnections could explain much of the local variability on monthly to interdecadal timescales. On the contrary, wind events with a minimum duration of a few hours are the focus of our study. Therefore, a proper assessment of the percentage of events modulated by large-scale pressure systems could be the topic of forthcoming studies. A further approach could be used to put our results in the context of large-scale processes. Besides the well-known weather type approach introduced by Lamb (1950), also James (2007) provides a full list of pressure systems which can cause the different wind events in our domain. On larger scale, the pressure systems could be classified according to the weather regimes defined by Hochman et al. (2021). Nevertheless, a proper application of such methods is beyond the scope of this paper.

The novelty of this study is to provide a full characterization of the wind patterns in the German Bight in terms of duration, magnitude, and seasonality, taking into account the differences deriving from the choice of the specific sites in the domain. We also provide a picture of the MSLP patterns which generate the local winds included in the catalog and show the relationship between the intensity and position of the pressure centers and the magnitude and seasonality of the detected events. The full catalog is available online (Rubinetti, 2023) and then can be used to select relevant events which can affect the local dynamics at specific locations in the German Bight.

The adopted methodology to identify and characterize the surface atmospheric conditions can be easily adapted to other research areas. It is important to highlight that this catalog derives from wind data extracted from single cells of the reanalysis data set, which is the common source of surface boundary data for the numerical simulations. As expected, it is characterized by biases—partly due to the resolution of the model (about 30 km at the considered latitudes)—which are significant especially during extreme events (see Kalverla et al., 2019, 2020); this fact must be considered when comparing the catalog provided here and the direct wind measurements. The next step could be evaluating the ocean response to all these events through high-resolution numerical simulations (Androsov et al., 2019; Fofonova et al., 2019; Kuznetsov et al., 2020). Such efforts are unavoidable to answer questions about the connectivity between different sites and to which extent the in situ long-term time series can describe the dynamics of a specific region.

### Data Availability Statement

This study has been conducted using ERA5 hourly data on single levels from 1959 to present provided by the Copernicus Climate Change Service, Climate Data Store (2023) (<https://doi.org/10.24381/cds.adbb2d47>). The wind catalog provided in this study is freely available online at the URL: <https://doi.org/10.5281/zenodo.7937439> (Rubinetti, 2023). All the maps shown in the main text and in Supporting Information S1 have been made with MATLAB *m\_map* package (Pawlowicz, 2020). In this study, the SOM package for MATLAB software, available from the Helsinki University of Technology (Finland) at the URL <http://www.cis.hut.fi/projects/somtoolbox>, was used (Vesanto et al., 1999, 2000). All the analyses have been performed with the MATLAB software.

### Acknowledgments

This study was funded by the German Federal Ministry of Education and Research (BMBF) in the frame of the joint research projects MGF-Nordsee (FKZ 03F0847A) and CREATE (03F0910B), parts of the research mission “Protection and Sustainable use of Marine Areas,” within the German Marine Research Alliance (DAM). We acknowledge support by the Open Access Publication Funds of Alfred-Wegener-Institut Helmholtz-Zentrum für Polar- und Meeresforschung. We thank the anonymous Reviewers for their detailed and helpful comments. Finally, SR thanks Dr. Sabine Horn for her support. Open Access funding enabled and organized by Projekt DEAL.

### References

- Androsov, A., Fofonova, V., Kuznetsov, I., Danilov, S., Rakowsky, N., Harig, S., et al. (2019). FESOM-C v.2: Coastal dynamics on hybrid unstructured meshes. *Geoscientific Model Development*, 12(3), 1009–1028. <https://doi.org/10.5194/gmd-12-1009-2019>
- Barnston, A. G., & Livezey, R. E. (1987). Classification, seasonality and persistence of low-frequency atmospheric circulation patterns. *Monthly Weather Review*, 115(6), 1083–1126. [https://doi.org/10.1175/1520-0493\(1987\)115<1083:CSAPOL>2.0.CO;2](https://doi.org/10.1175/1520-0493(1987)115<1083:CSAPOL>2.0.CO;2)
- Barriopedro, D., García-Herrera, R., Lupo, A. R., & Hernández, E. (2006). A climatology of Northern Hemisphere blocking. *Journal of Climate*, 19(6), 1042–1063. <https://doi.org/10.1175/JCLI3678.1>
- Bülow, K., Ganske, A., Heinrich, H., Hüttl-Kabus, S., Klein, B., Klein, H., et al. (2013). Comparing meteorological fields of the ENSEMBLES regional climate models with ERA-40-data over the North Sea. [https://doi.org/10.5675/kiwas\\_21.2013\\_era40data](https://doi.org/10.5675/kiwas_21.2013_era40data)
- Callies, U., Gaslikova, L., Kapitza, H., & Scharfe, M. (2017). German Bight residual current variability on a daily basis: Principal components of multi-decadal barotropic simulations. *Geo-Marine Letters*, 37(2), 151–162. <https://doi.org/10.1007/s00367-016-0466-2>
- Copernicus Climate Change Service (C3S) Climate Data Store (CDS). (2023). ERA5 hourly data on single levels from 1940 to present. <https://doi.org/10.24381/cds.adbb2d47>
- Donat, M. G., Leckebusch, G. C., Pinto, J. G., & Ulbrich, U. (2010). Examination of wind storms over Central Europe with respect to circulation weather types and NAO phases. *International Journal of Climatology*, 30(9), 1289–1300. <https://doi.org/10.1002/joc.1982>
- Feser, F., Barcikowska, M., Krueger, O., Schenk, F., Weisse, R., & Xia, L. (2015). Storminess over the North Atlantic and northwestern Europe—A review. *Quarterly Journal of the Royal Meteorological Society*, 141(687), 350–382. <https://doi.org/10.1002/qj.2364>
- Flanders Marine Institute. (2020). The intersect of the Exclusive Economic Zones and IHO seas areas, version 4. Retrieved from <https://doi.org/10.14284/402>
- Fofonova, V., Androsov, A., Sander, L., Kuznetsov, I., Amorim, F., Hass, H. C., & Wiltshire, K. H. (2019). Non-linear aspects of the tidal dynamics in the Sylt-Rømø Bight, south-eastern North Sea. *Ocean Science*, 15(6), 1761–1782. <https://doi.org/10.5194/os-15-1761-2019>
- Ganske, A., Tinz, B., Rosenhagen, G., & Heinrich, H. (2016). Interannual and multidecadal changes of wind speed and directions over the North Sea from climate model results. *Meteorologische Zeitschrift*, 25(4), 463–478. <https://doi.org/10.1127/metz/2016/0673>
- Guşatu, L. F., Menegon, S., Depellegrin, D., Zuidema, C., Faaij, A., & Yamu, C. (2021). Spatial and temporal analysis of cumulative environmental effects of offshore wind farms in the North Sea basin. *Scientific Reports*, 11(1), 10125. <https://doi.org/10.1038/s41598-021-89537-1>
- Hersbach, H., Bell, B., Berrisford, P., Hirahara, S., Horányi, A., Muñoz-Sabater, J., et al. (2020). The ERA5 global reanalysis. *Quarterly Journal of the Royal Meteorological Society*, 146(730), 1999–2049. <https://doi.org/10.1002/qj.3803>
- Hochman, A., Messori, G., Quinting, J. F., Pinto, J. G., & Grams, C. M. (2021). Do Atlantic–European weather regimes physically exist? *Geophysical Research Letters*, 48(20), e2021GL095574. <https://doi.org/10.1029/2021GL095574>
- Hurrell, J. W., & Deser, C. (2010). North Atlantic climate variability: The role of the North Atlantic Oscillation. *Journal of Marine Systems*, 79(3–4), 231–244. <https://doi.org/10.1016/j.jmarsys.2009.11.002>
- James, P. M. (2007). An objective classification method for Hess and Brezowsky Grosswetterlagen over Europe. *Theoretical and Applied Climatology*, 88(1), 17–42. <https://doi.org/10.1007/s00704-006-0239-3>
- Kalverla, P. C., Duncan, J. B., Jr., Steeneveld, G.-J., & Holtslag, A. A. M. (2019). Low-level jets over the North Sea based on ERA5 and observations: Together they do better. *Wind Energy Science*, 4(2), 193–209. <https://doi.org/10.5194/wes-4-193-2019>
- Kalverla, P. C., Holtslag, A. A. M., Ronda, R. J., & Steeneveld, G.-J. (2020). Quality of wind characteristics in recent wind atlases over the North Sea. *Quarterly Journal of the Royal Meteorological Society*, 146(728), 1498–1515. <https://doi.org/10.1002/qj.3748>
- Karagali, I., Peña, A., Badger, M., & Hasager, C. B. (2014). Wind characteristics in the North and Baltic Seas from the QuikSCAT satellite. *Wind Energy*, 17(1), 123–140. <https://doi.org/10.1002/we.1565>
- Kohonen, T. (1982). Self-organized formation of topologically correct feature maps. *Biological Cybernetics*, 43(1), 59–69. <https://doi.org/10.1007/BF00337288>
- Kohonen, T. (1997). *Self-organizing maps* (Vol. 30). Springer. <https://doi.org/10.1007/978-3-642-97966-8>



- Kuznetsov, I., Androsov, A., Fofonova, V., Danilov, S., Rakowsky, N., Harig, S., & Wiltshire, K. H. (2020). Evaluation and application of newly designed finite volume coastal model FESOM-C, effect of variable resolution in the southeastern North Sea. *Water*, *12*(5), 1412. <https://doi.org/10.3390/w12051412>
- Lamb, H. H. (1950). Types and spells of weather around the year in the British Isles: Annual trends, seasonal structure of the year, singularities. *Quarterly Journal of the Royal Meteorological Society*, *76*(330), 393–429. <https://doi.org/10.1002/qj.49707633005>
- Liu, Y., & Weisberg, R. H. (2011). A review of self-organizing map applications in meteorology and oceanography. In J. I. Mwasiagi (Ed.), *Self organising maps—Applications and novel algorithm design*. InTech. <https://doi.org/10.5772/13146>
- Liu, Y., Weisberg, R. H., & Mooers, C. N. K. (2006). Performance evaluation of the self-organizing map for feature extraction. *Journal of Geophysical Research*, *111*, C05018. <https://doi.org/10.1029/2005JC003117>
- Mailier, P. J., Stephenson, D. B., Ferro, C. A. T., & Hodges, K. I. (2006). Serial clustering of extratropical cyclones. *Monthly Weather Review*, *134*(8), 2224–2240. <https://doi.org/10.1175/MWR3160.1>
- Mathis, M., Elizalde, A., Mikolajewicz, U., & Pohlmann, T. (2015). Variability patterns of the general circulation and sea water temperature in the North Sea. *Progress in Oceanography*, *135*, 91–112. <https://doi.org/10.1016/j.pocean.2015.04.009>
- Mathis, M., & Pohlmann, T. (2014). Projection of physical conditions in the North Sea for the 21st century. *Climate Research*, *61*(1), 1–17. <https://doi.org/10.3354/cr01232>
- Montreuil, A.-L., Elyahyoui, J., & Chen, M. (2016). Effect of large-scale atmospheric circulation and wind on storm surge occurrence. *Journal of Coastal Research*, *75*(sp1), 755–759. <https://doi.org/10.2112/SI75-152.1>
- Pawlowicz, R. (2020). *M\_Map: A mapping package for Matlab*. University of British Columbia Earth and Ocean Sciences. [Online]. Retrieved from <http://www.eos.ubc.ca/rich/map.html>
- Pereira, D. (2022). *Wind rose*. MATLAB Central File Exchange. Retrieved from <https://de.mathworks.com/matlabcentral/fileexchange/47248-wind-rose>
- Quante, M., & Colijn, F. (Eds.). (2016). *North Sea region climate change assessment*. Springer International Publishing. <https://doi.org/10.1007/978-3-319-39745-0>
- Reusch, D. B., Alley, R. B., & Hewitson, B. C. (2007). North Atlantic climate variability from a self-organizing map perspective. *Journal of Geophysical Research*, *112*, D02104. <https://doi.org/10.1029/2006JD007460>
- Richardson, A. J., Risien, C., & Shillington, F. A. (2003). Using self-organizing maps to identify patterns in satellite imagery. *Progress in Oceanography*, *59*(2), 223–239. <https://doi.org/10.1016/j.pocean.2003.07.006>
- Rubineti, S. (2023). Data from “A complete 60-year catalogue of wind events in the German Bight (North Sea) derived from ERA5 reanalysis data” [Dataset]. Zenodo. <https://doi.org/10.5281/zenodo.7937439>
- Schmidt, H., & von Storch, H. (1993). German Bight storms analysed. *Nature*, *365*(6449), 791. <https://doi.org/10.1038/365791a0>
- Siegismund, F., & Schrum, C. (2001). Decadal changes in the wind forcing over the North Sea. *Climate Research*, *18*, 39–45. <https://doi.org/10.3354/cr018039>
- Sprong, P. A. A., Fofonova, V., Wiltshire, K. H., Neuhaus, S., Ludwichowski, K. U., Käse, L., et al. (2020). Spatial dynamics of eukaryotic microbial communities in the German Bight. *Journal of Sea Research*, *163*, 101914. <https://doi.org/10.1016/j.seares.2020.101914>
- Stanev, E. V., Badewien, T. H., Freund, H., Grayek, S., Hahner, F., Meyerjürgens, J., et al. (2019). Extreme westward surface drift in the North Sea: Public reports of stranded drifters and Lagrangian tracking. *Continental Shelf Research*, *177*, 24–32. <https://doi.org/10.1016/j.csr.2019.03.003>
- Sündermann, J., & Pohlmann, T. (2011). A brief analysis of North Sea physics. *Oceanologia*, *53*(3), 663–689. <https://doi.org/10.5697/oc.53-3.663>
- Sušelj, K., Sood, A., & Heinemann, D. (2010). North Sea near-surface wind climate and its relation to the large-scale circulation patterns. *Theoretical and Applied Climatology*, *99*(3), 403–419. <https://doi.org/10.1007/s00704-009-0149-2>
- Vesanto, J., Himberg, J., Alhoniemi, E., & Parhankangas, J. (1999). Self-organising map in Matlab: The SOM toolbox. In *Proceedings of the Matlab DSP conference* (Vol. 99, pp. 16–17). Espoo.
- Vesanto, J., Himberg, J., Alhoniemi, E., & Parhankangas, J. (2000). *SOM toolbox for Matlab 5, report A57*. Helsinki University of Technological.
- Walz, M. A., Donat, M. G., & Leckebusch, G. C. (2018). Large-scale drivers and seasonal predictability of extreme wind speeds over the North Atlantic and Europe. *Journal of Geophysical Research: Atmospheres*, *123*, 11518–11535. <https://doi.org/10.1029/2017JD027958>
- Wang, X. L., Wan, H., Zwiers, F. W., Swail, V. R., Compo, G. P., Allan, R. J., et al. (2011). Trends and low-frequency variability of storminess over Western Europe, 1878–2007. *Climate Dynamics*, *37*(11), 2355–2371. <https://doi.org/10.1007/s00382-011-1107-0>
- Wang, Z., & Liu, W. (2021). Wind energy potential assessment based on wind speed, its direction and power data. *Scientific Reports*, *11*(1), 16879. <https://doi.org/10.1038/s41598-021-96376-7>
- Weinert, M., Mathis, M., Kröncke, I., Pohlmann, T., & Reiss, H. (2021). Climate change effects on Marine Protected Areas: Projected decline of benthic species in the North Sea. *Marine Environmental Research*, *163*, 105230. <https://doi.org/10.1016/j.marenvres.2020.105230>
- Wiltshire, K. H., Kraberg, A., Bartsch, I., Boersma, M., Franke, H.-D., Freund, J., et al. (2010). Helgoland Roads, North Sea: 45 years of change. *Estuaries and Coasts*, *33*(2), 295–310. <https://doi.org/10.1007/s12237-009-9228-y>